Full Text View

Tropical Pacific Ocean Mixed Layer Heat Budget: The Pacific Cold Tongue

Mark S. Swenson

National Oceanic and Atmospheric Administration/Atlantic Oceanographic and Meteorological Laboratory, Miami, Florida

Donald V. Hansen

Cooperative Institute for Marine and Atmospheric Studies, University of Miami, Miami, Florida

ABSTRACT

Data from satellite-tracked drifting buoys and VOS/XBT profiles for the years 1979–95 were used to evaluate the seasonal cycle of how major oceanic processes redistribute heat in the cold tongue region of the tropical Pacific. The most active processes for the annual cycle are local heat storage and heat export by entrainment of upwelling and by mean meridional advection. Heat export by zonal advection, however, is not negligible, and meridional eddy heat fluxes associated with tropical instability waves effect a negative feedback that offsets a considerable fraction of that produced by the mean meridional advection. All of these processes mimic the essentially one cycle per year of the surface wind stress, as do those of the depths of both the bottom of the surface mixed layer and the thermocline. Because it is associated with poleward Ekman transports, upwelling, and baroclinic adjustment near the equator, the zonal wind stress component appears to be the more important. The meridional wind stress, while weaker in the annual mean, has a larger annual variation and, therefore, has equal influence on the annual variation of the scalar stress and perhaps the mixed layer thickness. The Monin–Obukov length is found to underestimate the mixed layer thickness considerably. Finally, the authors produce the first estimates of the seasonal cycle of eddy heat flux convergence, which plays a significant role in the evolution of the cold tongue, and show that the eddy heat flux convergence can be quantitatively modeled as eddy diffusion with a diffusivity derived from single-particle buoy statistics.

1. Introduction

The annual march of the ITCZ–cold tongue complex is of central importance to the evolution of the coupled ocean–atmosphere climate system in the American hemisphere and is a focus of the Pan American Climate Study (PACS) program. Although the basic facts of this annual march have been described (Mitchell and Wallace 1992), the processes that control the evolution of the pattern are subject to conjecture. Assessment of these processes is essential for identifying the physical mechanisms that must be included in predictive and diagnostic models, and for determining the variables to be monitored as necessary. Climatologically, the cold tongue is a recurrent feature of the surface waters of the eastern tropical Pacific Ocean. It is evident throughout the year with its strongest expression in September/October extending to the date line and its weakest expression in March confined near the coast (Sadler et al. 1987). A maximum transfer of heat into the ocean across the air–sea interface occurs in this region (Oberhuber 1988), so local oceanic processes must be important in redistributing heat in this region.

Two aspects of the annual average and seasonal cycles of oceanic and atmospheric conditions in the eastern tropical Pacific (and Atlantic) have attracted great interest. The first of these is the north–south asymmetry that arises because the intertropical convergence zone (ITCZ) of the atmosphere and the warmest ocean surface waters reside in the Northern Hemisphere year-round. The other is the observation that, in spite of a principally semiannual modulation of solar radiation at the top of the atmosphere in the deep Tropics, the seasonal cycle in these regions is primarily annual, essentially an extension of the seasons of the extratropical Southern Hemisphere. These general features and some of their more detailed attributes were described by Mitchell and Wallace (1992) who also suggested some hypotheses for their explanation. Wang (1994) and Nigam and Chao (1996) used EOF analyses with COADS to describe relationships among surface oceanic and atmospheric variables in more detail and in the context of basin and global-scale patterns, but were unable to identify causes of the special aspects of the region beyond making general assertions about the importance of air–sea–land surface coupling.

These couplings have been investigated in a sequence of model experiments by Chang (1994), Köberle and Philander (1994), Xie (1994), Xie and Philander (1994), Chang and Philander (1994), Li and Philander (1996), Philander et al. (1996), Chang (1996), and others. For efficiency of computation and interpretation of results, most of the coupled models have been built around reduced gravity ocean models that simulate the depth of the main thermocline, with or without a surface mixed layer incorporated within the upper layer. These models suggest the influence of various dynamic and geographic factors but must be considered with caution because of the necessarily very abbreviated physics included.

We focus on the ocean mixed layer heat budget of the cold tongue region in the Pacific. An overview of the considerations was given by Enfield (1986). In recent investigations, Hayes et al. (1991) and Bond and McPhaden (1995) used relatively local and short-term measurements from moored buoys and research vessels to illuminate these issues. The eastern equatorial Pacific has two rather different regimes that are distinguished by the direction of prevailing winds along the equator. The easterly regime, west of approximately 110°W, is characterized by prevailing easterly winds and an associated strong equatorially symmetric upwelling signature. The southerly regime, east of about 110°W, is characterized by prevailing southerly winds and a more diffuse cold SST signature centered south of the equator near 1°S. We base our investigation of the easterly regime on over a decade (1979–95) of measurements from satellite-tracked drifting buoys and volunteer observing ships in the region. This extends eastward into the southerly regime because we did not want the heavily occupied XBT line at 110°W (Fig. 1 ⊙, bottom) to lie on the boundary of our study region. Our region is centered on the equator and, because drifters tend to diverge from the equator in this region, the poleward limits are the narrowest for which adequate drifter data are available. As our study is based on the heat budget integrated over the region, we consider the pattern of the seasonal cycle, but not the cross-equatorial asymmetry.

In the following section we describe the logical basis of our analysis and the measurements used for its implementation. Details of the analysis procedure are described in section 3, followed by primary results and some discussion of them in terms of the regional oceanography. Subsequent papers are planned to present results of a parallel analysis to the adjacent but quite different region of the North Equatorial Countercurrent and apply these results to evaluation of surface heat flux climatologies.

2. Approach and data

The budget equation for conservation of heat in the ocean surface mixed layer can be expressed as

$$Q_0 - Q_h = \rho C_p \left\{ h \frac{D_H \Theta}{Dt} + \Delta T W_e \right\}, \qquad (1)$$

in which Q_0 and Q_h are the downward heat flux across the top and bottom of the surface mixed layer, ρC_p is the heat capacity per unit volume of seawater, h is the mixed layer thickness, Θ is the vertically averaged temperature of the mixed layer, D_H/Dt is a horizontal operator, W_e is the entrainment, or upwelling velocity at the bottom of the mixed layer, and ΔT is the difference between Θ and the temperature just below the mixed layer. In this paper we focus on terms on the right-hand

side (rhs) of (1), that is, upon the disposition by ocean processes within the mixed layer of heat exchanged across its surface and bottom boundaries. The entrainment velocity W_e is estimated as

$$W_e = \frac{\partial h}{\partial t} + \mathbf{\nabla}_H(h\mathbf{V}_H), \qquad (2)$$

where $\mathbf{V}_H$ is the vertically averaged horizontal velocity of the mixed layer and $\mathbf{\nabla}_H$ is a horizontal operator. The derivation of (1) follows Stevenson and Niiler [1983, Eq. (3)], except that we have changed notation and neglected the term that involves the correlation of the departures of horizontal velocity and temperature from their vertically averaged values. This term is not available from our data (as it was not from those of Stevenson and Niiler) and may be nontrivial. We judge that it is of minor importance in the region (see the appendix).

The substantial or Lagrangian derivative within the first term on the rhs of (1) expresses the temperature change experienced at a point moving with the vertically averaged motion of the surface mixed layer. It is alternatively expressed and most commonly used in the form

$$\frac{D_H\Theta}{Dt} = \frac{\partial\Theta}{\partial t} + \mathbf{V}_H \cdot \mathbf{\nabla}_H\Theta \qquad (3)$$

and can be positive or negative depending upon the signs and magnitudes of the other processes represented in (1). The second term on the rhs of (1) quantifies the effect on the heat budget of warming by an amount ΔT the water that is entrained across the bottom of the mixed layer. The entrained water partially balances the divergent part of the mixed layer flow with the difference associated with changes in the mixed layer depth (2).

Although our development does not explicitly invoke a slablike mixed layer, our conclusions require the assumption that the mean temperature of the mixed layer can be adequately characterized by a temperature measurement taken just below the surface. Likewise, we must suppose that the mean velocity of the mixed layer can be characterized by the movements of a drifter, which follow a drogue that extends over a range of about 6 m centered on 15-m depth. It is hard to justify these assumptions because slablike mixed layers are seldom seen in nature, but this type of mixed layer model has been a useful idealization in oceanography for many years and it is hard to imagine an observation-based study of this kind that could overcome this limitation.

Measurements of water movements and temperature required to evaluate the processes expressed in (1) were obtained from satellite-tracked drifting buoys operated in the region of the cold tongue for the EPOCS and Tropical Oceans Global Atmosphere (TOGA) programs during 1979–1995. The earliest measurements were made using FGGE-type buoys attached to subsurface drogues centered at 35-m depth (Hansen and Paul 1984, 1987). From late 1981 onward, drogue depths were standardized to 15 m. From early 1984 to 1987 smaller buoys with improved water following properties (Bitterman and Hansen 1986) were deployed. After early 1988, and for by far the greater part of the measurements, the WOCE/TOGA standard drifter has become the design of choice. Whereas the earliest drifters could not be certified as following water movements with accuracy better than about 5 cm s^{-1}, the WOCE/TOGA drifter has been calibrated for an accuracy of <1 cm s^{-1} for conditions prevailing in the cold tongue region (Niiler et al. 1995). All buoys were equipped with drogue-loss sensors of various designs, and we use only data from buoys reporting attached drogues in this study.

Sea surface temperatures were measured at a submerged point of the hull from all of the buoys. These temperature measurements have a precision of about 0.1°C (Bitterman and Hansen 1993) and a standard deviation of about 0.3°C (Reynolds and Smith 1994). We use these measurements to estimate Θ. This is generally a very good approximation and, in any case, a small bias for individual buoys will not affect our results because most of the computations required involve derivatives rather than absolute temperatures. Estimates of Θ and $D_H\Theta/Dt$ were derived only from measurements made between 0000 and 0600 local time to avoid contamination from the diurnal cycle of superficial warming. Hence, the buoy data provide accurate information about $\mathbf{V}_H$ and $D_H\Theta/Dt$ for the mixed layer, except possibly very near the equator when upwelling is particularly strong and in immediate proximity to the equatorial front (Wyrtki 1981) during periods of energetic tropical instability wave activity.

Buoys released prior to mid-1987 transmitted continuously, to be received during local satellite passes five to six times a day. Subsequently, and for the preponderance of data, buoys were programmed for reduced transmissions to reduce cost (Hansen and Poulain 1996). Several duty cycles were used, but the most common and most sparse was for continuous transmissions during one day of three.

An estimate of the Lagrangian correlation time is required to estimate the effective number of (independent) data. For

midlatitude oceans, the decorrelation time has been estimated as six to nine days for zonal currents and three to seven days for meridional components (Krauss and Böning 1987; Poulain and Niiler 1989; Thomson et al. 1990; Swenson and Niiler 1996). This parameter is less well known for the tropical oceans, but Hansen and Paul (1984), Hansen and Herman (1989), and Bi and Niiler (1998) suggest ranges of 10 to 15 days for zonal currents and 3 to 10 days for meridional currents. The usual approach to estimate the integral timescales has been to integrate the velocity autocorrelations for which convincing evidence of convergence usually is lacking and datasets are usually small. Indeed, Sanderson and Booth (1991) suggest that a true decorrelation scale for the ocean is not to be found, at least on the time and space scales observed to date. We assume that a useful approximation to the correlation scales relevant to our application can be estimated. To make use of the large drifting buoy dataset now available for the cold tongue region, we fit the rational quadratic function $[K_\infty T^2(T + T_{corr})^{-1}]$ to the three- and six-day structure function values given for the equatorial band (3°S to 7°N) by Hansen and Poulain (1996). The longitudinal structure function is calculated from the residuals after subtracting a mean zonal flow of 23 cm s^{-1} (Reverdin et al., 1994). The fitted function, for which T denotes variable time lag, K_∞ the long-time diffusivity, and T_{corr} the correlation time (twice the Lagrangian integral timescale), is conditionally negative-definite and, therefore, appropriate for modeling variance (Christakos 1984). It reproduces the short and long time asymptotic behavior described by Taylor (1921) and interpolates smoothly between them. Fitting to statistical parameters derived from the large dataset for the equatorial Pacific yields T_{corr} = 5 days for latitude and 14 days for longitude. The associated values of K_∞ are 1.3×10^4 m^2 s^{-1} and 6.6×10^4 m^2 s^{-1}, respectively.

The same logic can be applied to obtain the Lagrangian correlation scale for measurements of temperature change ($D_H\Theta/Dt$) from Lagrangian structure functions for surface temperature. Hansen and Herman (1989) and Hansen and Poulain (1996) show that, if the diurnal cycle of surface temperature is filtered, the structure function for the several-day variations is linear, as for Brownian motion, expressing loss of correlation on timescales shorter than a day. Hence, we elected to base computations of velocity components and temperature changes on double transmission duty cycle (six day) changes of location and surface temperature as suggested by Hansen and Herman (1989). This procedure gives measurement errors of less than 0.1 cm s^{-1} for velocity components and 3×10^{-7} K s^{-1} for temperature changes and provides independent measurements for $D_H\Theta/Dt$ and meridional velocity, and about twofold redundance for zonal velocity.

The quality-controlled XBT dataset of Donoso et al. (1994) was used to determine the mixed layer depths required for evaluation of terms in (1). Various definitions of the "mixed layer" are extant in the literature. One extreme is exemplified by Stevenson and Niiler (1983) who used the depth to an isotherm as much as several degrees less than the SST to obtain mixed layer depths on the order of 100 m in the cold tongue extension into the central Pacific. The other extreme is exemplified by Bond and McPhaden (1995) who define the depth of the bottom of the mixed layer as the depth at which the temperature is 0.1 K less (or the potential density 0.01 kg m^{-3} greater) than at the sea surface, resulting in mixed layers as thin as 10 m at 140°W on the equator. We require a definition of the mixed layer that is at once sufficiently macroscopic and robust to be estimated reliably from XBT profile data and for which the current measurements by drifting buoys provide an accurate characterization. Interpretation of results is facilitated when the bottom of the mixed layer is chosen deep enough to obviate concerns about the microphysical processes associated with diurnal variations within the macroscale mixed layer and for a large part of the shortwave radiation penetrating the ocean surface to be absorbed within the mixed layer. Results from Lewis et al. (1990) and Siegel et al. (1995) suggest that, on average, about 90% of the incident shortwave radiation is absorbed in the upper 40 m of the ocean in the cold tongue region. After some study of the XBT profile data available, we chose the same criterion as used by Lamb (1984) for the tropical Atlantic, and by Rao et al. (1989) for the tropical Indian Ocean, to define the mixed layer. The bottom of the mixed layer is taken to be the depth at which the temperature is 1 K less than that at the shallowest recorded depth (typically about 3 m). Mixed layer depths were estimated from individual XBT profiles by linear interpolation between the shallowest depth that exceeded the 1-K criterion and the adjacent shallower recorded depth.

Parameterization of the cooling by entrainment in terms of the temperature "jump" ΔT seems to have been introduced by Ball (1960) for modeling the atmospheric surface boundary layer and has subsequently been used for many ocean mixed layer models and diagnostics as well (cf. Kraus and Turner 1967; Stevenson and Niiler 1983; Seager et al. 1988; Hayes et al. 1991; Chang 1994). Although this parameterization is appealingly simple, quantification of ΔT is ambiguous in application to actual mixed layer data. Various artifices have been used to estimate ΔT. Some of the results imply entrainment from a level twice or more as deep as the bottom of the mixed layer, and some seem to allow the possibility of $\Delta T < 0$, implying heating of the mixed layer by entrainment, but are not explicit about it. For an ideal mixed layer defined by a temperature difference δT in a continuous temperature profile, ΔT logically must be equal to δT. Real temperature profiles rarely fit the ideal model exactly. If the criterion is applied to a poorly formed mixed layer consisting of a constant gradient, then $\Delta T = \frac{1}{2}\delta T$ (because ΔT is defined relative to the average temperature of the mixed layer). If the temperature profile in the mixed layer is concave upward, $\Delta T > \frac{1}{2}\delta T$ and, conversely, if the profile is convex upward. In application to observed temperature profiles, ΔT may thus be seen as an expression of the quality, or approach to an ideal mixed layer, of the profile. The archived XBT data are inadequate to support such distinctions. We have chosen to use $\Delta T = 0.75$ K because it seems to be of appropriate magnitude and causes the annual cycle of entrainment cooling to exactly mimic that of W_e. This value is not to be confused

with the numerically equal dimensionless constant introduced by Seager et al. (1988), and used also by Chang (1994), for example, without explanation. A more extensive study of the vertical heat flux processes currently under way suggests that ΔT varies seasonally, but that is beyond the scope of the present analysis.

Time and space scales of thermal variability have been considered numerous times over the past two decades. A most recent and detailed evaluation of particular pertinence to the cold tongue is that of Kessler et al. (1996). For variations of depth of the 20°C isotherm, which we expect to be similar to those of the mixed layer, at 110°W they estimated zonal and meridional integral (to the first zero-crossing of the cross correlation) length scales of about 1300 and 175 km for high-frequency variations. A typical volunteer observing ship (VOS) from which most of our XBT data are obtained travels at about 18 knots and makes XBT profile observations four times per day, or at intervals of about 200 km, mostly at large crossing angles to the equator. About 15% of these profiles were rejected as unsuitable for estimates of the bottom of the mixed layer. The VOS return time is much longer than the integral timescale (about five days over the entire tropical band). On the basis of their meridional and temporal separation, we take the XBT profile data to be independent.

3. Analysis procedure

The overall distribution of drifting buoy and XBT measurements are shown by Fig. 1 . For each of the fields h, Θ, U, V, and $D_H\Theta/Dt$, data from all years were composited by month, and means and standard deviations were computed for each calendar month. The monthly data location centroids varied less than $3/4°$ latitude and 4° longitude from $1/4°$N, 112°W, so we do not expect variability of sampling location to introduce errors. Figure 2 depicts estimates of the means and the associated standard errors for each field while Table 1 provides the means and standard deviations in tabular form.

The annual cycle of the regional mean mixed layer temperature (Fig. 2a) has a simple annual cycle with maximum and minimum in April and September, respectively, joined by intervals of nearly constant rate of temperature change. The maximum (minimum) mean eastward zonal velocity (Fig. 2b) occurs a month or less prior to that of temperature. The apparent small average meridional velocity results from its near symmetry about the equator and is not at all expressive of its importance to the heat budget as will be seen. The mean mixed layer depth (Fig. 2c) has a simple but asymmetric annual cycle with a well-defined minimum near 25 m in March/April and a vaguely defined maximum near 50 m in the autumn. All of these variables mimic, in a general way, the seasonal variation of the local surface wind stress (Fig. 2e). Mitchell and Wallace (1992) and Nigam and Chao (1996), among others, have attempted to evaluate the relative importance of zonal and meridional wind stresses for generation of the cold tongue. Locally, the zonal wind stress is about 50% larger in the mean and the meridional component has about 50% larger annual range, but their phasing is nearly coincident. Because the meridional component of current is strongly asymmetric about the equator (to be shown), its monthly mean values over this region centered on the equator are too small and variable to reveal a clear annual cycle. Its average over the full year is essentially zero. The annual cycle of Lagrangian temperature change (Fig. 2d) is particularly interesting and enigmatic. Aside from the aberrant value for March, which perhaps is attributable to a relatively, but not uniquely, modest number of observations, it consists of two distinct modes. During autumn and winter it holds near 5×10^{-7} K s^{-1}, while during spring/summer it holds at about -1×10^{-7} K s^{-1}. Abrupt transitions between these states occur during March/April and August/September. The aberrant value for $D_H\Theta/Dt$ in March leads to similar aberrations in subsequent computations. With careful study we have been unable to identify any systematic defect in the March observations.

To capture the spatial patterns that give rise to heat flux divergence associated with spatial covariances between the variables, the data were normalized to unit variance after subtracting the monthly means and fit to the truncated orthogonal basis set:

$$f(x, y, t) = \text{Re}\left\{ \sum_{i=0}^{1} \sum_{j=0}^{3} \sum_{k=0}^{2} X_i(x)Y_j(y)Z_k(t) \right\}, \quad (4)$$

where X_i and Y_j are the set of polynomials (unnormalized Legendre polynomials) $S_0(\eta) = 1$, $S_1(\eta) = \eta$, $S_2(\eta) = 3\eta^2 - 1$, $S_3(\eta) = (5/3)\eta^3 - \eta$, orthogonal on the range $-1 \leqslant x \leqslant 1$, with $x = (\lambda - 114°\text{W})/15°$, and $y = \Phi/4°$, λ and Φ being longitude and latitude. Here Z_l are the set of harmonics, $Z_l = \exp(i2l\pi\omega)$, where ω = one cycle per year. We retained only functions whose fits accounted for at least 4% of the remaining variance to obtain

$$+ \; \Theta_3 S_1(x)\}, \tag{5b}$$

$$U(y, t) \rightarrow \langle U \rangle_k + \sigma_{Uk}$$

$$\times \left\{ U_1 S_3(y) + U_2 S_2(y) \cos\frac{\pi}{2}\left(\frac{k}{3} - \frac{1}{2}\right)\right\}, \tag{5c}$$

$$V(y, t) \rightarrow \langle V \rangle_k + \sigma_{Vk} V_1 S_1(y), \tag{5d}$$

$$\frac{D_H\Theta}{Dt} \rightarrow \left\langle \frac{D_H\Theta}{Dt}\right\rangle_k, \tag{5e}$$

in which $\langle \; \rangle_k$ and $\sigma_{(\;)_k}$ denote the mean and standard deviation of the respective variables for month k. Notice that the solution in the form (5c) requires algebraic manipulation from the form (4) and that the phase factor of $\pi/3$ is an approximation that is in error by less than 2%. Equations (5) provide a concise expression of the climatology of several mixed layer parameters in the cold tongue region. These fitted parameters are provided in Table 2 O=.

The expressions (5) account, in order, for 32%, 65%, 31%, 10%, and 5% of the variances in the original data, and we cannot discern any spatial patterns in the residuals. The small fraction of variances in V and $D_H\Theta/Dt$ captured by these representations is due to large variations associated with both interannual and submonthly timescales. For V, the latter consists primarily of mesoscale currents associated with tropical instability waves (TIW). When TIW are well developed, strong thermal fronts also develop, and surface buoys can be towed across these fronts by the subsurface drogues in the vertically sheared currents, which leads to large values of $D_H\Theta/Dt$. This process is suggested by the observation (not shown) that the most extreme values of $D_H\Theta/Dt$ occur in the eastern half of the Northern Hemisphere part of the region and in the second half of the year when TIW are best developed. Although most of the data are from buoys well designed and calibrated for measuring horizontal currents, the buoys are quasi-Lagrangian in the sense that they cannot follow three-dimensional motions. Fortunately, enough measurements have now been accumulated that climatological patterns can be seen despite the noise caused by these processes.

Several expected or notable features are apparent from Eq. (5). The core of the thermal tongue is displaced south of the equator and the mean mixed layer depth is symmetric about the equator to this level of approximation (Fig. 1 O=). The annual mean zonal velocity (Fig. 3 O=) displays the expected minimum south of the equator in the westward South Equatorial Current (SEC). The SEC reverses during the spring, during which time there is an eastward maximum south of the equator. The meridional current is simply antisymmetric about the equator, and no spatial pattern emerges for $D_H\Theta/Dt$. These figures closely resemble corresponding analyses (Reverdin et al. 1994; GDC 1995) of large subsets of the same drifter dataset using 1° by 25° longitude and 2° latitude by 8° bin averaging, but of course smoothed as expected by the low-order polynomial representation.

Quantification of (2) in terms of monthly ensemble averages does not account for eddy fluxes that arise from higher frequency correlations between the velocity and the SST gradients. Direct estimates of these fluxes are not possible with our data and approach. After multiplication by h, as in (1), the eddy fluxes are dominated by $h\langle \mathbf{V}'_H \Theta' \rangle$, in which primes denote temporal deviations that are strongly filtered from monthly averages, but other deviation products appear as well. The principal source of such deviations in this region is tropical instability waves that have been shown to produce a strong meridional eddy heat flux (Hansen and Paul 1984; Philander et al. 1986). We evaluated the eddy heat flux as

$$\langle \mathrm{EF} \rangle_k = \rho C_p \langle h \rangle_k \left\{ \left\langle \frac{D_H\Theta}{Dt}\right\rangle_k - \left\langle \frac{\partial\Theta}{\partial t}\right\rangle_k \right.$$

$$\left. - \langle \mathbf{V}_H \rangle_k \cdot \langle \nabla_H \Theta \rangle_k \right\}. \tag{6}$$

Being calculated as a residual, EF must be expected to have relatively large uncertainty.

Products appearing in (1), (2), and (6) were formed using expressions (5) and averaged over the region to obtain estimates for the seasonal cycle of each of the terms of the heat budget. $\partial h/\partial t$ and $\partial \Theta/\partial t$ were calculated as a centered difference. Errors were estimated using standard rules (Meyer 1975) for propagation of error through the calculations. The greatest uncertainty associated with these estimates is that arising from the possible, but unknown, interplay between interannual variations and nonuniform sampling.

4. Results

The annual cycles of zonal and meridional volume transport divergence, which together with a term proportional to $\partial h/\partial t$ complete the estimate of entrainment into the mixed layer (2), are shown in Fig. 4 ⬤. The horizontal divergence is dominated by the meridional term, which, due to the coupling between meridional velocity and mixed layer thickness, increases threefold, while the zonal wind stress less than doubles between the vernal and autumnal equinoxes (Fig. 2e ⬤). Notice that the volume or mass transport of the mixed layer as used here is not synonymous with Ekman transport. This is not surprising for a region encompassing the equator. The horizontal divergence agrees with that inferred for this general region from earlier drifting buoy measurements (Hansen and Paul 1987; Poulain 1993), but is about four times larger than that found by Bryden and Brady (1985) for the upper 100 m of a somewhat larger overlapping region. The difference is probably attributable to the greater layer depth considered in the latter study, which includes the meridional convergence of the geostrophic flow that is expected below the wind-driven mixed layer. In February, when the mixed layer thins rapidly, the magnitude of $\partial h/\partial t$ approaches the minimum values of $\partial(hV)/\partial y$, but for most of the year it is similar to that of $\partial(hU)/\partial x$. Due primarily to the magnitude of $\partial(hV)/\partial y$, it is evident that W_e is positive (upward) in all monthly averages, so that detrainment is of no concern in our analysis. Although the zonal surface current is nondivergent and is constant over the region, the geographical variations of mixed layer depth give rise to spatial structure in both components of the volume transport divergence.

The central results of our investigation, the seasonal cycle of the contribution of several oceanic processes to the heat transport divergence in the cold tongue, are illustrated in Fig. 5 ⬤. The largest contribution to the mean annual export from the region (58 W m^{-2}) is by meridional advection (Fig. 5a ⬤), which ranges from over 100 W m^{-2} in September to less than 20 W m^{-2} in March. Zonal advection (Fig. 5a ⬤) is less important in the annual mean (24 W m^{-2}), but exhibits a large annual variation from 70 W m^{-2} in August to zero, or evenly slightly less, in April. These advective contributions arise from both the mean advection and the eddy heat flux as discussed last section. The eddy heat flux (Fig. 5c ⬤), although subject to large uncertainty because it is derived as the residual from the other processes, is clearly negative, providing a convergence of heat into the core of the cold tongue. Its magnitude in the annual mean (42 W m^{-2}) is comparable to that required to heat water entrained from below (Fig. 5b ⬤) and its annual range is comparable to that of mean meridional advection (not shown). The phase of the eddy heat flux is in opposition to that of meridional advection, however, so that it serves to moderate the heat flux from mean meridional advection throughout the year. This has been noted before (Hansen and Paul 1984; Philander et al. 1986; Flament et al. 1996), but our study provides the first quantitative depiction of the seasonal cycle.

The export of heat by the warming of the water entrained into the mixed layer from below (Fig. 5b ⬤) is positive throughout the year and is substantial in the annual mean (46 W m^{-2}), with extremes of 70 W m^{-2} in August and 15 W m^{-2} in February. These estimates contain the uncertainty associated with the poorly constrained choice for ΔT. A different positive value or a seasonally varying value will change the magnitudes but not the sign of the heat loss arising from entrainment.

Notice that the advection entrainment and eddy heat flux divergence processes shown in Fig. 5 ⬤ all have an annual cycle that mimics those of the local wind stress, with a predominantly annual harmonic structure that exhibits extremes in March or April and August or September. The two stress components are so similar in their seasonal cycle that it is difficult to discriminate between their effects on the basis of their relative phasing. The meridional stress component is weaker than the zonal component in all months of the year, but its seasonal modulation is some 50% larger and the seasonal modulation relative to the annual mean is about two and a half times larger, which supports the suggestion by Mitchell and Wallace (1992) of a major role for meridional stress in determining the annual cycle of SST.

Figure 5d ⬤ is especially revealing. It shows the monthly evolution of the full rhs of Eq. (1) and the annual cycle of local heat storage, which carries the sign of SST tendency. The difference between these two curves is the net monthly export of heat by mean advective and horizontal eddy processes. We see that, generally speaking, the export of heat by advective and horizontal eddy processes is small during February through April and large and steady from May through January. After April (Phase I of Mitchell and Wallace 1992), the cold tongue begins to develop at the expense of heat storage as ocean export increases while solar radiance and net surface heat flux are decreasing (Oberhuber 1988). By October, the cold tongue has reached its strongest expression and the temperatures in the mixed layer begin to rise despite the continued

export of heat by ocean advection and horizontal eddy processes through January. This indicates that the vertical transport processes that we do not observe are serving to import heat to the mixed layer during this period. Certainly, less penetrative radiation will exit the bottom of the mixed layer during October through January when the mixed layer is relatively deep (Fig. 2c). There is considerable uncertainty in the seasonal cycle of net downward surface heat flux. The National Centers for Environmental Prediction (NCEP) reanalysis (Kalnay et al. 1996), for example, is about 40 W m^{-2} greater than that of Oberhuber (1988) during July through January. Finally, the seasonal cycle of cooling associated with vertical turbulent heat transport through the bottom of the mixed layer is very poorly known, but it may decrease during the warming phase of the cold tongue.

Overall, the ocean exports heat from the region at an annual average rate of about 85 W m^{-2}, ranging from a maximum of about 150 W m^{-2} in September to a minimum of about 15 W m^{-2} during late winter/early spring (discounting the large value for March). The uncertainty attached to these estimates is considerably smaller than would be obtained by summing the advective and eddy components shown in Fig. 5 because the sum of these processes is measured directly in $D_H\Theta/Dt$. For comparison, the Oberhuber (1988) atlas, which is typical of similar recent atlases based on the in the region, indicates an annual average net surface heat flux of about 80 W m^{-2}, extrema near 110 W m^{-2} in February and 50 W m^{-2} in June. The agreement of our annual mean rate of heat export with that from Oberhuber (1988) is not as good as these numbers would suggest because the net surface heating must be corrected for heat loss through the bottom of the mixed layer by penetrative radiation and turbulent flux. There is ample range (±60 W m^{-2}) in local heat storage (Fig. 5d) to supply the seasonal differences between net surface flux and the oceanic export, but there are some discrepancies of phasing. Further investigation of the nature and source of this discrepancy is under way. The magnitude of the seasonal cycle of heat storage in the mixed layer (Fig. 5d) relative to that of surface heating (Oberhuber 1988) is a priori evidence that local oceanic processes are important in redistributing heat in the mixed layer in this region.

The second term on the rhs of (1) may be influenced by correlations of eddy fluctuations of velocity and mixed layer thickness, which in the absence of simultaneous measurements we cannot evaluate. This is unlikely to be important, however, because the detailed description given by Flament et al. (1996) of the structure of eddies associated with tropical instability waves shows little evidence of the asymmetry that would produce an eddy-induced vertical mass flux.

5. Discussion

Studies of the heat budget require careful consideration of ambiguities that can be introduced by the arbitrary choice of a reference point for temperature, which is often made implicitly. In our treatment, this potential problem is avoided because we make use of only derivatives and differences of temperature. An alternative determination of the heat budget could be calculated from the heat flux across the defining boundaries of the control volume, as was done by Wyrtki (1981), Bryden and Brady (1985), or Enfield (1986). Such calculations are properly done only across sections of zero net mass transport (Montgomery 1974). We may interpret our results in terms of the conceptual model implied by these alternative determinations of the heat budget. If the defining lateral boundaries are zonal and meridional, the results can be interpreted in terms of zonal and meridional circulation cells if the entrainment mass and heat fluxes are partitioned between zonal and meridional components in proportion to their respective divergences (Fig. 4). Because the meridional component of the mass or volume flux is much larger than the zonal component, most of the heat flux required for the warming of entrained water will be counted in the meridional cell, and the zonal result will differ little from $\rho C_p hU\Theta_x$ (Fig. 5a). The picture that emerges, therefore, assigns a dominant role for the classic model of meridional divergence and upwelling. These undergo similar seasonal cycles (Figs. 5a and 5b) and are minimum in February and maximum in August/September.

Interest has been expressed in the relative importance of local upwelling in the cold tongue versus water upwelled at the coast farther east in maintaining the cold tongue. Equation (1) provides a novel way of considering this question. Inasmuch as the heat export required to warm the vertical entrainment is explicitly contained in the second term on the rhs of (1), $\rho C_p hD_H\Theta/Dt$ can be considered to represent the heating of waters from geographically adjacent regions as they are advected through. During most of the year, the South Equatorial Current provides a strong westward flow into our study region, so it is natural to think that the first term on the rhs of (1) (which we will refer to as "Lagrangian heating") represents the influence of the coastal upwelling region to the east. This interpretation perhaps would be more compelling if our analysis region had been selected to extend right to the coast. We believe, however, that the region shown in Fig. 1 is sufficiently representative of the cold tongue that such changes of extent or location are unlikely to engender qualitative changes in our results. This interpretation implies that significant changes of mixed layer temperature in the region are accomplished by both local upwelling and from horizontal advection of coastally upwelled water, but that these processes have quite different seasonal cycles (Fig. 5b). Heating of locally upwelled water absorbs heat in all months of the year and mimics the annual cycle of wind stress in the eastern equatorial Pacific, being minimal in February and a maximum in August through December. This appears to be a result of wind-induced upwelling and entrainment. The annual cycle of Lagrangian heating of water moving through the region is at once more variable and enigmatic. It has two phases: September through March when heat absorption and export is very high and relatively steady at about 75 W m^{-2}, and April through August when it

reverses sign and imports heat to the cold tongue. The onset of this second phase occurs in March/April when the SEC reverses, the wind stress is minimum, the mixed layer temperature is maximum, and the mixed layer is very thin (Fig. 2 ⊙). During the following months the advective import continues to supply some of the heat required for heating water entrained into the mixed layer as the wind stress and zonal current increase and the mixed layer cools and thickens. By September, all of these variables are at or near their annual extremes, and as wind stress diminishes, Lagrangian heating switches to its export mode.

The annual extrema of SST and wind stress along the northern coast of Peru precede those in our cold tongue region by one to two months, in February and August/September (Stricherz et al. 1992). Might the heat transport modes observed in the cold tongue be attributable to advection of conditions observed in the coastal upwelling regime at an earlier time? The center of our study region is about 3500 km from the coast of South America. Projecting the zonal current speeds (Fig. 2a ⊙) to the coast yields an estimated travel time of about three months. Thus, the calculation of heat import or export to the cold tongue is consistent with the idea of relatively warm or cold water being advected from a coastal source. The sharpness of the switching between modes remains unexplained, however. The uncertainties associated with estimation of the seasonal cycle are too large to permit a strong conclusion about the robustness of these rapid transitions between import and export modes, but the possibility merits further consideration.

The spring switch from Lagrangian heat export to heat import occurs during phase I of the transition from warm to cold seasons as described by Mitchell and Wallace (1992). During their phase II (May to August) there is little change to the Lagrangian mode, but heating of locally entrained water increases steadily (Fig. 5b ⊙). Mitchell and Wallace (1992) describe a seasonal evolution of the cold-tongue/ITCZ that they suggest is triggered by the strengthening of remote zonal winds or of local meridional winds, favoring the latter. Both these conceptual models are rooted in numerical model experiments that diagnosed the response of thermocline depth to wind.

As noted in the introduction, various assumptions have been made about the nature of the surface mixed layer and its relation to the depth of the thermocline for model-based investigations. In several model studies of air–sea interaction mechanisms, a mixed layer of constant depth has been assumed. Figures 1 ⊙ and 2 ⊙ and Tables 1 ⊙ and 2 ⊙ show that this is not a good approximation, as our observations demonstrate that the mixed layer thickness varies by a factor of 2 in both time and space. As emphasized by Chen et al. (1994a), mixed layer depth is of particular importance not only because thin mixed layers are more conducive to surface cooling by wind-induced upwelling but, more importantly, because the mixed layer thickness determines the volume or mass over which the net surface heat flux comes to be distributed. Thus, in our computations, although the month to month changes of mixed layer thickness have little influence on estimation of W_e (cf. Fig. 4 ⊙), the factor of 2 difference in mixed layer depth between spring and autumn has a major effect on the SST tendency ($=\partial\Theta/\partial t$) associated with Q_o. Also, relatively thin but variable mixed layer thickness such as occurs in the cold tongue region can be associated with substantial and variable heat loss to the mixed layer by penetrative shortwave radiation, and quite possibly turbulent transport as well.

Figure 6 ⊙ reiterates Fig. 2c ⊙, the monthly mean cycle of mixed layer thickness for our study region, for comparison with that of the 20°C isotherm depth extracted from the same XBT data. The 20°C isotherm occurs near the center of the main or permanent thermocline and is commonly used as the indication for thermocline depth. By this measure it is seen that the thermocline is well below the bottom of the mixed layer in all months, but its seasonal modulation is only slightly less and so similar in its evolution that its use in lieu of a more appropriate mixed layer in a simple model might easily be compensated by modest changes in other model parameters.

Another length scale of importance for mixed layer modeling is the generalized Monin–Obukov length,

$$L = \rho C_p u^3_*/\alpha g Q_o, (7)$$

in which $u* = (\tau/\rho,)^{1/2}$ α is the thermal expansion coefficient for seawater, g is the gravitational acceleration, τ is the magnitude of the wind stress, and other symbols are defined earlier. Equation (7) expresses a ratio of turbulent kinetic energy creation by surface wind stress to turbulent kinetic energy suppression by conversion to potential energy. At equilibrium the mixed layer depth is supposed to be proportional to L, but estimates of the constant of proportionality vary greatly, evidently because (7) is only a partial model of the physical processes involved (see Gargett et al. 1979 for a summary). A more general form of (7) was developed by Kraus and Turner (1967) for estimation of mixed layer thickness and temperature and variations on this general theme have been used in numerous other model studies. Xie (1994) uses a variation to model entrainment velocity into a mixed layer of fixed thickness, and Chang (1994) and Chen et al. (1994a) reported that use of the Kraus and Turner model in modified form lead to realistic SST simulations. Monthly mean values of L were computed from the Stricherz et al. (1992) wind stress data and net surface heat flux values from the NCEP/NCAR reanalyses (Kalnay et al. 1996) and are shown also in Fig. 6 ⊙. It can be seen that L typically is only about 15% or so of the mixed layer depth. If the effect of surface freshwater exchange on potential energy of the mixed layer is included in its calculation, L will become even smaller around the time of the vernal equinox, and only slightly larger during autumn. We interpret this result to indicate that processes not directly connected to the local wind stress, such as shear instabilities in

tropical instability waves, are important contributions to turbulent kinetic energy in the region. Although divergence of the zonal component of velocity (Fig. 4 ⊙) contributes trivially in our computation of entrainment, the strong zonal currents may be another important mechanism for generation of turbulence via shear instability and, therefore, have major implication for both entrainment velocity and mixed layer depth. Chen et al. (1994b), whose mixed layer model includes such shear instability for production of turbulent kinetic energy, suggest that this is a characteristic of tropical oceans generally.

It has been shown (Figs. 5a,c ⊙) that the nominal meridional heat flux, $\rho C_p h V \partial \Theta / \partial y$, is largely offset by the meridional eddy heat flux. The sum of these two terms is highly variable as expected. About all that can be said usefully is that the meridional advection is larger in the annual mean by about 16 ± 7 W m^{-2}, and eddy heat flux is the larger by about 15 W m^{-2} in only two months (February and August). If the appropriate fraction of heat flux by entrainment is added to the meridional advection as mentioned previously, then the upwelling–meridional circulation limb significantly exceeds the eddy feedback in all seasons. We expect that the rhs of Eq. (1) (Fig. 5d ⊙) should bear fair resemblance to the seasonal cycle of Q_o given by surface heat flux atlases. Some comparisons to net surface heat flux values from Oberhuber (1988) and the NCEP/NCAR reanalyses (Kalnay 1996) reveal that they are similar to our results in the annual mean and contain a predominantly annual harmonic with phase similar to that of Fig. 5d ⊙. The range of annual variation from our results is considerably larger, however. Some of this discrepancy can be attributed to heat flux out the bottom of the mixed layer by penetrative shortwave radiation and turbulent flux. Also, although the cooling by entrainment process has been used extensively in mixed layer modeling, assignment of a temperature for the entrained water is anything but rigorous, and perhaps can be improved.

It is of interest also to see how well the annual cycle of the EF found in section 4 can be modeled as diffusion of heat using the diffusivity determined in section 2 from drifting buoy statistics. In terms of the variables of (4), the divergence of diffusive heat flux is

$$\text{DEF} = -\rho C_p h K \Theta_{yy}$$
$$= -5.0 \times 10^{-5} K \langle h \rangle_k \sigma_{\Theta k} \text{ W m}^{-2} \qquad (8)$$

[note that from (4), $\Theta_{xx} = 0$]. We take $K_\infty = 1.3 \times 10^4$ m^2 s^{-1} to be the annual average diffusivity and are guided by the result of Taylor (1921) and the suggestion of Hansen and Swenson (1996) that the seasonal cycle of diffusivity can be modeled by the variance of the meridional velocity component. Thus, we assume

$$K_k = \frac{12\sigma_{uk}^2}{\sum_k \sigma_{uk}^2} \times 1.3 \times 10^4 \text{ m}^{-2} \text{ s}^{-1}. \qquad (9)$$

The result of calculating DEF using (7) in (6) is plotted in Fig. 5c ⊙. These results are consistent with the evolution of the meridional component of instability wave energy at (1°S–1°N, 140°W) from June 1990 to June 1991, where the energetic period extends from August through December and the quiet period extends from January through June (Qiao and Weisberg 1995).

In summary, it appears impossible to ascribe an inconsequential role to any of the oceanographic processes represented in the rhs of (1) or (3). The most important advective process is meridional, but that is moderated by substantial meridional eddy flux by TIW. Zonal currents have substantial direct influence on the export of heat and quite likely on mixed layer depth by production of turbulence, both directly and via the intermediary of TIW.

REFERENCES

Ball, K. F., 1960: Control of inversion height by surface heating. *Quart. J. Roy. Meteor. Soc.,* **86,** 483–494..

Bi, K., and P. P. Niiler, 1998: The equatorial Pacific responses to 1991–1992 ENSO as observed with Lagrangian mixed layer drifters. *J. Geophys. Res.,* in press..

Bitterman, D. S., and D. V. Hansen, 1986: The design of a low-cost tropical drifter buoy. *Proc. Marine Data Systems International Symp.,* New Orleans, LA, Mar. Technol. Soc., 575–581..

—— , and —— , 1993: Evaluation of surface temperature measurements from drifting buoys. *J. Atmos. Oceanic Technol.,* **10,** 88–96..

Bond, N. A., and M. J. McPhaden, 1995: An indirect estimate of the diurnal cycle in the upper ocean turbulent heat fluxes at the equator, 140°W. *J. Geophys. Res.,* **100** (C9), 18 369–18 378..

Bryden, H. L., and E. C. Brady, 1985: Diagnostic model of the three-dimensional circulation in the upper equatorial Pacific Ocean. *J. Phys. Oceanogr.,* **15,** 1255–1273.. Find this article online

Chang, P., 1994: A study of the seasonal cycle of sea surface temperature in the tropical Pacific Ocean using reduced gravity models. *J. Geophys. Res.,* **99** (C4), 7725–7741..

—— , 1996: The role of dynamic ocean–atmosphere interactions in the tropical seasonal cycle. *J. Climate,* **9,** 2973–2985.. Find this article online

—— , and S. G. H. Philander, 1994: A coupled ocean–atmosphere instability of relevance to the seasonal cycle. *J. Atmos. Sci.,* **51,** 3627–3648.. Find this article online

Chen, D., A. J. Busalacchi, and L. M. Rothstein, 1994a: The roles of vertical mixing, solar radiation, and wind stress in a model simulation of the sea surface temperature seasonal cycle in the tropical Pacific Ocean. *J. Geophys. Res.,* **99** (C10), 20 345–20 359..

—— , L. M. Rothstein, and A. J. Busalacchi, 1994b: A hybrid vertical mixing scheme and its application to tropical ocean models. *J. Phys. Oceanogr.,* **24,** 2156–2179.. Find this article online

Christakos, G., 1984: On the problem of permissible covariance and variogram models. *Water Resour. Res.,* **20,** 251–265..

Donoso, M. C., J. E. Harris, and D. B. Enfield, 1994: Upper ocean thermal structure of the eastern tropical Pacific. DOC/NOAA Tech. Rep., ERL-450-AOML 36, 221 pp. [NTIS PB95171781.].

Enfield, D. B., 1986: Zonal and seasonal variations of the near-surface heat balance of the equatorial Pacific Ocean. *J. Phys. Oceanogr.,* **16,** 1039–1054.. Find this article online

Flament, P., S. Kennan, R. Knox, P. Niiler, and R. Bernstein, 1996: The three-dimensional structure of an upper ocean vortex in the tropical Pacific Ocean. *Nature,* **383,** 610–613..

Gargett, A. E., T. B. Sanford, and T. R. Osborn, 1979: Surface mixing layers in the Sargasso Sea. *J. Phys. Oceanogr.,* **9,** 1090–1111.. Find this article online

Global Drifter Center, 1995. Comparison of TOGA tropical Pacific Ocean model simulations with the WOCE/TOGA Surface Velocity Programme drifter data set. WOCE/TOGA Surface Velocity Programme Planning Committee/Numerical Experimentation Group: World Climate Research Programme. [Available from Global Drifter Center, Scripps Institution of Oceanography, University of California, San Diego, 9500 Gilman Dr., La Jolla, CA 92093-0230.].

Hansen, D. V., and C. A. Paul, 1984: Genesis and effects of long waves in the equatorial Pacific. *J. Geophys. Res.,* **89** (C11), 10 431–10 440..

—— , and —— , 1987: Vertical motion in the eastern equatorial Pacific inferred from drifting buoys. *Oceanol. Acta,* No. SP, 27–32..

—— , and A. Herman, 1989: Temporal sampling requirements for surface drifting buoys in the tropical Pacific. *J. Atmos. Oceanic Technol.,* **6,** 599–607..

—— , and P.-M. Poulain, 1996: Quality control and interpolations of WOCE-TOGA drifter data. *J. Atmos. Oceanic Technol.,* **13,** 900–909..

—— , and M. S. Swenson, 1996: Mixed layer circulation during EqPac and some thermochemical implications for the equatorial cold tongue. *Deep-Sea Res. II,* **43** (4–6), 707–724..

Hayes, S. P., P. Chang, and M. J. McPhaden, 1991: Variability of the sea surface temperature in the eastern equatorial Pacific during 1986–1988. *J. Geophys. Res.,* **96** (C6), 10 553–10 566..

Kalnay, E., M. Kanamitsu, R. Kistler, W. Collins, D. Deaven, L. Gandin, M. Iredell, S. Saha, G. White, J. Woollen, Y. Zhu, M. Chelliah, W. Ebisuzaki, W. Higgins, J. Janoiak, K. C. Mo, C. Ropelewski, J. Wang, A. Leetmaa, R. Reynolds, R. Jenne, and D. Joseph, 1996: The

NCEP/NCAR 40-Year Reanalysis Project. *Bull. Amer. Meteor. Soc.,* **77,** 437–471.. Find this article online

Kessler, W. S., M. C. Spillane, M. J. McPhaden, and D. E. Harrison, 1996: Scales of variability in the equatorial Pacific inferred from the tropical atmosphere ocean buoy array. *J. Climate,* **9,** 2999–3024.. Find this article online

Köberle, C., and S. G. H. Philander, 1994: On the processes that control seasonal variations of sea surface temperatures in the tropical Pacific Ocean. *Tellus,* **46A,** 481–496..

Kraus, E. B., and J. S. Turner, 1967: A one-dimensional model of the seasonal thermocline. *Tellus,* **19,** 98–105..

Krauss, W., and C. W. Böning, 1987: Lagrangian properties of eddy fields in the northern North Atlantic as deduced from satellite-tracked buoys. *J. Mar. Res.,* **45,** 259–291..

Lamb, P. J., 1984: On the mixed-layer climatology of the north and tropical Atlantic. *Tellus,* **36A,** 292–305..

Lewis, M. R., M.-E. Carr, G. C. Feldman, W. Esaias, and C. McClain, 1990: Influence of penetrating solar radiation on the heat budget of the equatorial Pacific Ocean. *Nature,* **347,** 543–545..

Li, T., and S. G. H. Philander, 1996: On the annual cycle of the eastern equatorial Pacific. *J. Climate,* **9,** 2986–2998.. Find this article online

Meyer, S. L., 1975: *Data Analysis for Engineers and Scientists,* John Wiley and Sons, 513 pp..

Mitchell, T. P., and J. M. Wallace, 1992: The annual cycle in equatorial convection and sea surface temperature. *J. Climate,* **5,** 1140–1156.. Find this article online

Montgomery, R. B., 1974: Comments on "seasonal variability" of the Florida Current, by Niiler and Richardson. *J. Mar. Res.,* **32** (3), 533–534..

Nigam, S., and Y. Chao, 1996: Evolution dynamics of tropical ocean-atmosphere annual cycle variability. *J. Climate,* **9,** 3187–3205.. Find this article online

Niiler, P. P., A. S. Sybrandy, K. Bi, P. M. Poulain, and D. S. Bitterman, 1995: Measurements of the water-following capability of holey-sock and TRISTAR drifters. *Deep-Sea Res.,* **42,** 1951–1964..

Oberhuber, J. M., 1988: *An Atlas Based on the "COADS" Data Set:The Budgets of Heat, Buoyancy and Turbulent Kinetic Energy at the Surface of the Global Ocean.* Max Planck Institute for Meteorology Rep. 15, Max-Planck-Institute für Meteorologie, Hamburg, Germany. [Available from Max-Planck-Institut für Meteorologie, Bundesstraße 55, D-2000 Hamburg 13, Germany.].

Philander, S. G. H., W. J. Hurlin, and R. C. Pacanowski, 1986: Properties of long equatorial waves in models of the seasonal cycle in the tropical Atlantic and Pacific Oceans. *J. Geophys. Res.,* **91** (C12), 14 207–14 211..

—— ,D. Gu, D. Halpern, G. Lambert, N.-C. Lau, T. Li, and R. C. Packanowski, 1996: Why the ITCZ is mostly north of the equator. *J. Climate,* **9,** 2958–2972.. Find this article online

Poulain, P.-M., 1993: Estimates of horizontal divergence and vertical velocity in the equatorial Pacific. *J. Phys. Oceanogr.,* **23,** 601–607.. Find this article online

—— ,and P. P. Niiler, 1989: Statistical analysis of the surface circulation in the California Current system using satellite-tracked drifters. *J. Phys. Oceanogr.,* **19,** 1588–1603.. Find this article online

Qiao, L., and R. H. Weisberg, 1995: Tropical instability wave kinematics: Observations from the Tropical Instability Wave Experiment. *J. Geophys. Res.,* **100,** 8677–8693..

Rao, R. R., R. L. Molinari, and J. F. Festa, 1989: Evolution of the climatological near-surface thermal structure of the tropical Indian Ocean. 1. Description of the mean monthly mixed layer depth, and sea surface temperature, surface current, and surface meteorological fields. *J. Geophys. Res.,* **94** (C8), 10 801–10 815..

Reverdin, G., C. Frankignoul, E. Kestenave, and M. J. McPhaden, 1994: Seasonal variability in the surface currents of the equatorial Pacific. *J. Geophys. Res.,* **99** (C10), 20 323–20 344..

Reynolds, R. W., and T. M. Smith, 1994: Improved global sea surface temperature analyses using optimum interpolation. *J. Climate,* **7,** 929–948.. Find this article online

Sadler, J. C., M. A. Lander, A. M. Hori, and L. K. Oda, 1987: *Tropical Marine Climatic Atlas,* V. II: *Pacific Ocean.* UHMET 87-02, University of Hawaii, Department of Meteorology, 27 pp..

Sanderson, B. G., and D. A. Booth, 1991: The fractal dimensions of drifter trajectories and estimates of horizontal diffusivity. *Tellus,* **43A,**

334–349..

Seager, R., S. E. Zebiak, and M. A. Cane, 1988: A model of the tropical Pacific sea surface temperature climatology. *J. Geophys. Res., 93,* 1265–1280..

Siegel, D. A., J. C. Ohlman, L. Washburn, R. R. Bidigare, C. T. Nosse, E. Fields, and Y. Zhou, 1995: Solar radiation, phytoplankton pigments and the radiant heating of the equatorial Pacific warm pool. *J. Geophys. Res., 100* (C10), 4885–4891..

Stevenson, J. W., and P. P. Niiler, 1983: Upper ocean heat budget during the Hawaii to Tahiti Shuttle Experiment. *J. Phys. Oceanogr., 13,* 1894–1907.. Find this article online

Stricherz, J., J. J. O'Brien, and D. M. Legler, 1992: *Atlas of Florida State University Tropical Pacific Winds for TOGA, 1966–1985.* Florida State University, 250 pp..

Swenson, M. S., and P. P. Niiler, 1996: Statistical analysis of the surface circulation of the California Current. *J. Geophys. Res., 101* (C10), 22 631–22 645..

Taylor, G. I., 1921: Diffusion by continuous movements. *Proc., London Math. Soc., 20,* 196–211..

Thomson, R. E., P. H. LeBlond, and W. J. Emery, 1990: Analysis of deep-drogued satellite-tracked drifter measurements in the northeast Pacific. *Atmos.-Ocean, 28* (4), 409–443..

Wang, B., 1994: On the annual cycle in the tropical eastern central Pacific. *J. Climate, 7,* 1926–1942.. Find this article online

Wilson, W. D., and A. Leetmaa, 1988: Acoustic Doppler radar current profiling in the equatorial Pacific in 1984. *J. Geophys. Res., 93,* 13 947–13 966..

Wyrtki, K., 1981: An estimate of equatorial upwelling in the Pacific. *J. Phys. Oceanogr., 11,* 1205–1214.. Find this article online

Xie, S.-P., 1994: On the genesis of the equatorial annual cycle. *J. Climate, 7,* 2008–2013.. Find this article online

—— ,and S. G. H. Philander, 1994: A coupled ocean–atmosphere model of relevance to the ITCZ in the eastern Pacific. *Tellus, 46A,* 340–350..

APPENDIX

6. Evaluation of Heat Flux Divergence by Profile Structure Covariance

Consider the heat flux divergence associated with covariance between the vertical profiles of temperature and velocity. Intuitive considerations based upon Ekman theory and the typical thermal stratification of the tropical oceans suggest that the zonal component of the covariance is generally negative in the South Equatorial Current, but give little help as to even the sign of its divergence. The meridional component is expected, on average, to be negative in the Northern Hemisphere and positive in the Southern Hemisphere. It is, therefore, divergent at the equator, but of unknown magnitude.

To look further into the significance of this term, we obtained Doppler current profiler and XBT data collected during cruises of the NOAA Ship *Researcher* for the EPOCS program (Wilson and Leetmaa 1988). Current profiling was done between 3°N and 3°S on 110°W during April, June, October, and November 1984 and along the equator from 155° to 90°W in November 1984. Doppler current profiles were averaged over lengths of ship track that were 28 km meridionally and 50 km zonally. An XBT profile was available at the middle of each length. The profiles of velocity and temperature were averaged vertically between the sea surface and the bottom of the mixed layer and departures from these averages computed. The integral $\int_{-h}^{0} \mathbf{V}'T'\, dz$ was evaluated using the trapezoidal rule. The covariance values from the zonal and meridional sections were then differenced along the meridional and zonal sections, divided by the mixed layer depth times the separation distance and averaged along each section. Considerable differences, but no systematic pattern, emerged among the four meridional sections, so these data were folded together. The resulting values of temperature transport were −0.05 ± 0.04 K per month for the meridional component, and 0.04 ± 0.03 K per month for the zonal component of this process. One hundred or more profile pairs went into each of these calculations, indicating that the variance is indeed large, even when velocity observations are averaged over tens of kilometers. Nonetheless, these results suggest that the heat flux associated with covariance between the vertical profiles of temperature and velocity is about 10% (or less) of the other terms in (1).

Tables

Table 1. Monthly means and standard deviations. Numbers in parentheses indicate standard deviations.

	Θ (°C)	$D_H\Theta/Dt$ (10^{-2} °C da^{-1})	h (m)	U (cm s^{-1})	V (cm s^{-1})
Jan	25.3 (1.24)	3.56 (5.05)	52.0 (23.1)	−11.9 (25.5)	−3.19 (19.4)
Feb	26.1 (0.91)	2.72 (6.26)	33.8 (18.3)	−30.4 (22.8)	−3.97 (15.0)
Mar	27.0 (1.03)	6.66 (6.17)	24.3 (12.7)	−33.1 (37.5)	2.90 (17.1)
Apr	27.6 (1.03)	−0.46 (9.26)	26.1 (13.1)	15.7 (37.0)	−1.32 (13.4)
May	26.9 (1.06)	−1.03 (8.27)	35.0 (12.4)	3.6 (37.7)	3.85 (14.7)
Jun	26.1 (1.42)	−1.01 (10.26)	38.4 (16.3)	−15.7 (36.3)	2.10 (23.6)
Jul	24.9 (1.59)	−0.50 (10.88)	40.4 (16.6)	−30.1 (36.5)	1.91 (19.7)
Aug	24.3 (2.15)	−0.48 (13.33)	47.7 (23.3)	−47.2 (37.6)	−5.32 (22.6)
Sep	23.3 (1.87)	3.81 (12.43)	46.8 (16.9)	−39.7 (40.3)	1.16 (24.7)
Oct	23.7 (1.99)	4.19 (8.73)	42.2 (21.2)	−26.6 (31.8)	0.06 (20.7)
Nov	24.4 (1.60)	3.18 (9.42)	53.6 (23.1)	−36.6 (31.3)	3.50 (19.6)
Dec	24.6 (1.39)	2.96 (8.61)	45.2 (28.3)	−29.4 (30.5)	−1.60 (20.5)

Click on thumbnail for full-sized image.

Table 2. Function fit parameters.

| H_1	H_2	Θ_1	Θ_2	Θ_3	U_1	U_2	V_1
0.275	−0.432	0.453	0.389	−0.574	1.27	0.314	0.589

Click on thumbnail for full-sized image.

Figures
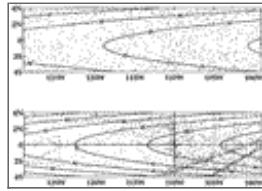
Click on thumbnail for full-sized image.

Fig. 1. Top: Geographical distribution of drifter observations superimposed on the annual mean SST pattern determined by the fit given by Eq. (4b). Bottom: Geographical distribution of XBT observations superimposed on the annual mean mixed layer depth pattern determined by the fit given by Eq. (4a).
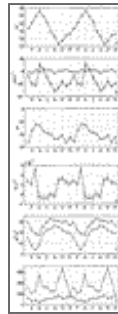
Click on thumbnail for full-sized image.

Fig. 2. Monthly means and standard errors for (a) SST, (b) zonal (O) and meridional (✳) velocity, (c) mixed layer depth, and (d) $D_H\Theta/Dt$. Panel (e) is the seasonal cycle of westward (O) and northward (✳) psuedostress (m^2 s^{-2}) (Stricherz et al., 1992). Panel (f) depicts the number of samples for drifters (O) and XBTs (✳).
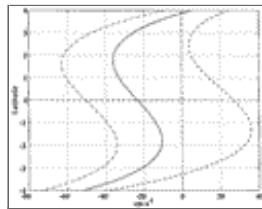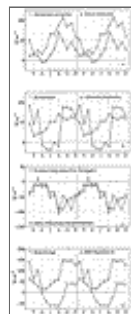

Click on thumbnail for full-sized image.

Fig. 3. Meridional structure of the fitted zonal velocity in the cold tongue region. Solid: Annual mean. Dash: Monthly mean for April. Dash–dot: Monthly mean for August. April and August represent the extremes of the seasonal cycle (see Fig. 2 ⬤).

Fig. 4. Monthly mean estimates of the components of mixed layer transport divergence and change of thickness: $(\partial/\partial x)hU$ (O), $(\partial/\partial y)hV$ (◇), and $\partial h/\partial t$ (✶). The mean of the estimated monthly standard errors are 12, 26, and 2, respectively, all $\times 10^{-7}$ m s^{-1}. The vertical axis on the right side provides the impact on the heat budget of these terms in watts per square meter with monthly standard errors of 12, 26, and 2 W m^{-2}, respectively.

Fig. 5. Monthly means of heat budget processes: (a) $\rho C_p hU\partial\Theta/\partial x$ (O) and $\rho C_p hV\partial\Theta/\partial y$ (✶); (b) $\rho C_p hD\Theta/Dt$ (O) and $\rho C_p \Delta T(\partial h/\partial t + \nabla_H \cdot (hV))$ (✶); (c) residual eddy heat flux (EHF) (✶) and $\rho C_p hK\partial^2\Theta/\partial y^2$ (O); and (d) $\rho C_p h\partial\Theta/\partial t$ (✶) and rhs of Eq. (1) (O). Estimates of standard errors are: (a) 8 and 26 W m^{-2}, respectively; (b) 18 and 12 W m^{-2}, respectively; (c) 34 W m^{-2} for the EHF; and (d) 7 and 23 W m^{-2}, respectively.
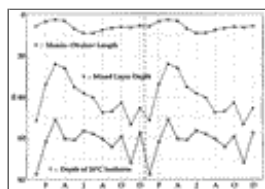
Fig. 6. Annual cycle of Monin–Obukov length (see text), mixed layer depth, and depth of the 20°C isotherm based on data from 1979–1995 in the region 4°S–4°N, 129°–99°W.

Corresponding author address: Dr. Mark S. Swenson, NOAA/AOML, 4301 Rickenbacker Causeway, Miami, FL 33149.

E-mail: swenson@aoml.noaa.gov

top ▲